Construction and Building Materials 367 (2023) 130342

Contents lists available at ScienceDirect

Construction and Building Materials

journal homepage: www.elsevier.com/locate/conbuildmat

Air granulated basic Oxygen furnace (BOF) slag application as a binder: Effect on strength, volumetric stability, hydration study, and environmental risk

M. Jawad Ahmed *, Winnie Franco Santos *, H.J.H. Brouwers

Department of Built Environment, Eindhoven University of Technology, Eindhoven, the Netherlands

ARTICLE INFO

Keywords:
Basic oxygen furnace (BOF) slag
Air granulated
Cement replacement
Supplementary cementitious material (SCM)
Leaching

ABSTRACT

This study evaluates the air granulated BOF slag potential as a cementitious material by comparing the granulated and conventionally cooled slags. The mechanical performance of the cement-slag composites is correlated with the hydration behaviour through thermal, mineralogical, and microstructural analysis. The findings show that the granulation improved the grindability, reactivity, and compressive strength till 28 days. The ~5% slag can be substituted as a binder and ~35% as an inert filler. The performance decline upon 20–50% replacements is attributed to the absence of brownmillerite reactivity. Overall, the granulation did not improve the cement-slag composite performance significantly till 90 days.

1. Introduction

Climate change due to anthropogenic CO_2 emissions is a critical challenge of this century. Among the CO_2 emission sources, the cement industry contributes 7–8% of anthropogenic CO_2 emissions and 26% of the industrial carbon emissions globally [1,2]. The worldwide cementitious material partners with the global cement and concrete association (GCCA), the International Energy Agency (IEA) and the Cement Sustainability Initiative (CSI) have set out several road maps aiming to be carbon neutral by 2050 [3–6]. In Europe, the two main construction sectors release 10% of total European CO_2 emissions. The cement industry produces 5% of CO_2 emissions while the same amount is contributed by the steel used in construction [7]. The UN Environment (2015) report "Eco-Efficient types of cement" identifies the two main routes that can promise CO_2 reduction in relatively short term as mitigation for emissions. Route number one is to increase the clinker substitution by supplementary cementitious material (SCM). And the second one is the more efficient use of cement in the downstream products such as mortars, concrete, etc. [8].

Basic oxygen furnace (BOF) slag is the by-product of the basic oxygen converter steel-making slag. Per each ton of steel generation, 90–110 kg of BOF slag is produced [9]. In Europe, the total production of steel furnace slag was 15.7 Mt in 2018. Out of all steel furnace slags, the BOF slag accounts for 52.7% of the total steel furnace slags in Europe [10,11]. A small portion of BOF slag is recycled in many countries while a high percentage is directly stacked or discarded occupying land resources. To reduce its dumping capacity, the residues are partially recycled for low-end applications in the construction industry mainly as aggregates [12,13]. Moreover, the potential leaching of heavy metals especially Cr and V can cause pollution to the surrounding water and soil [14]. Considering the rate at which natural resources are depleting, and the tremendous quantity of steel slag available, it is of great importance to recycle steel slag as an efficient building material to reduce its environmental impact [15–17].

The recycling and reuse of BOF slag carry many challenges [18,19]. Several strategies have been reported to improve the BOF slag valorization, such as mineral modification, carbonation, weathering, mechanical and alkali activation as well as high-temperature curing [20–23]. In particular, efforts are made to valorize BOF slag as fine aggregates for the development of geopolymer based materials (high-end application) by mixing it with other waste streams such as fly ash, mine tailings and blast furnace slag [24–29]. Moreover, the maximum ~5% replacement as an alternative to blast furnace slag in cement production exhibited a promise for high-end application [30,31]. But no profound economical application has been reported yet. BOF slag contains dicalcium silicate (35–45 wt%) and brownmillerite (20–30 wt%), mineralogically similar in phase composition to ordinary Portland cement (OPC) [32]. This makes BOF slag an ideal candidate for the

* Corresponding authors.
E-mail addresses: m.ahmed@tue.nl (M. Jawad Ahmed), w.franco.santos@tue.nl (W. Franco Santos).

https://doi.org/10.1016/j.conbuildmat.2023.130342
Received 3 August 2022; Received in revised form 30 December 2022; Accepted 5 January 2023
Available online 12 January 2023

replacement of clinker, and this approach can reduce the CO_2 emissions of limestone dissociation by up to 72.28 kg/t and coal combustion by up to 24.16 kg/t [33]. But several technical problems, such as the intensification of clinkering reactions due to steel slag addition, discourage this application. The steel slag has a significant inhibiting effect on the early age hydration of the cement via prolonging the induction period and uncertainty in setting time. The inhibition mechanism is attributed to low pH in pore solution due to steel slag addition in cement as well as depletion of gypsum further decrease the ettringite formation and inhibits the calcium silicate hydrate (C—S—H) precipitation [34].

One strategy to enhance the slag reactivity is changing the cooling process from slow to relatively faster cooling by granulation to prevent crystallization. This strategy has already been successfully utilized to improve the pozzolanic potential of blast furnace slag [35]. The air granulation of BOF slag provides a promising way to recover heat from the slag that has a tapping temperature between 1250 and 1700 °C [36]. The current industrial practice is pouring steel slag into large pits and cooling it with a continuous water stream. A few studies have investigated the impact of changing cooling process and speed on the mineralogical composition of BOF slag [37,38]. The studies have concluded that the fast cooling did not generate significant amorphous content but decreased the crystallite size and stabilize the reactive polymorphs of the slag phases that would contribute toward the high reactivity of BOF slag [37]. Nevertheless, some important questions need to be addressed systematically, such as to what extent the air granulation enhances the hydration potential of BOF slag relative to the conventionally cooled slag? Does air granulation exhibit more compatibility with OPC? Moreover, can the utilization of air granulated BOF slag as a filler improve the performance better than inert filler?.

To address all the above questions and evaluate the possible fast cooling impact on the cementitious properties of the BOF slag, the air granulated and conventional cooled BOF slags were applied as a replacement for OPC in mortar. To the author's best knowledge, there is no direct information reported about this comparative application study of air granulation and conventional cooled BOF slag as a replacement for cement. Furthermore, the hydration study of the cement-slag pastes is investigated for a better understanding of the possible cement-slag reaction.

The current study investigates the potential of air granulated BOF slag as an OPC replacement in the mortar and compares it with conventional cooled BOF slag. Moreover, the quartz powder was added with the same degree of replacement to compare the performance of the material with an inert material. The workability, mechanical performance, dimension stability, and environmental risk of 5, 20, 35, and 50% replacement clusters of OPC with slag as well as quartz powder were analysed over time. In addition to that, the thermal, mineralogical and microstructure analysis of cement-slag paste samples of the mortars was evaluated to understand the hydration behaviour for the novel binder application. Finally, the correlation between the chemical bound water of cement-slag pastes and the strength development of mortars as well as the potential leaching of heavy metals were investigated.

2. Materials and methods

2.1. Materials preparation and characterization

BOF slag taken from regular production at Tata Steel Europe in IJmuiden was cooled in two different ways: air granulated and conventional cooled at Harsco Metals Holland B.V. [39]. The slag is granulated at Harsco Metals Holland B. V. in a make-shift experimental facility by pouring in front of a strong air fan at a tapping temperature of 1592 ± 40 °C. While one part of the molten slag is cooled conventionally by pouring the liquid slag into pits and cooling it using water. Both conventional cooled (CSS) and air granulated BOF slag (GSS) were produced from the same batch of production to avoid possible variations in elemental oxide composition. The exact cooling rate during granulation is unknown and dependent on granule size. A detailed flow chart is shown in Fig. 1 to follow the steps taken for material preparation and characterization.

For larger slag granules, the cooling takes longer than for smaller granules of BOF slag. For this reason, the GSS received was sieved and divided into the following size fractions: >4 mm (3.8 wt%), 2–4 mm (47.2 wt%), 1–2 mm (39 wt%), 0.5–1 mm (6.5 wt%), 0.25–5 mm (0.7 wt %) and < 0.25 mm (2.8 wt%). Moreover, the quartz powder (QP) was used as an inert material and for the type of ordinary Portland cement (OPC) selected as a reference binder (REF), CEM-I 42.5N (ENCI Heidelberg cement) was chosen. The sample labelling has been shown in Table 1.

The CSS was received in cobble size (64–256 mm) as shown in Fig. 2 (a) and, with the help of a jaw crusher model BB2 (Retsch), reduced to sand size. After crushing, the CSS was also sieved between 0.25 and 8 mm to achieve the same particle size distribution (PSD) of GSS, aiming to have the granulometry of both materials as a fixed parameter for further comparison. Fig. 2(b) presents the conventionally cooled slag after crushing, with angular and laminar shape, rich in finer particles produced from the crushing process, while (c) presents the air granulated slag as received, in the form of spheres.

Representative aliquots of 1 kg (0.25–8 mm) were taken from CSS and GSS by using the static sample splitter, and ground using a Retsch RS 300 XL disc mill for 20 min at a constant speed of 912 per minute. A constant input of 1 kg was added in a grinding jar volume of 2 l.

2.1.1. Particle size distribution

The PSD of both slags was determined using Mastersizer 2000 from Malvern and the milled sample was dispersed in isopropanol. To understand the impact of specific surface area (SSA) on the hydration kinetics, the nitrogen adsorption (Tristar II 3020V1.03 series micrometer) at 77 K was measured using BET (Brunauer-Emmett-Teller) methods. The PSD and SSA have been presented in Fig. 3(a, b). Both slag distribution was designed and milled to have a similar size as a controlled parameter. Even having the same range of slag feed (0.25 to 8 mm) before milling, the air granulated slag exhibited a higher specific surface area (0.84 m^2/g) than conventionally cooled slag (0.63 m^2/g) after milling. The air granulation improves the grindability of slag.

The specific density of the materials is tested by a Helium pycnometer (AccuPyc II 1340). The sample labelling and density are presented in Table 1.

2.1.2. Oxide composition

Mass change was measured via heating slag samples at 1000 °C for 2 h. The chemical oxide composition was determined with X-ray - fluorescence (XRF; PANalytical Epsilon 3, standardless) using fused beads. The oxide composition of the raw material has been presented in Table 2. The GSS and CSS samples contain a high amount of Fe_2O_3 (~27 wt%) and MgO (~8wt%) than CEM I 42.5 N sample Fe_2O_3(~4 wt%). The GSS and CSS exhibited a mass gain (negative value of a loss on ignition) due to the conversion of ferrous oxide into ferric oxide. Moreover, the GSS also exhibited a little lower value of mass gain of 0.02 wt% than CSS (0.1 wt%) which indicates that the GSS sample is partially oxidized due to air granulation of the BOF slag.

2.1.3. Mineralogy of raw material

X-ray powder diffractograms were acquired using a Bruker D2 and D4 diffractometer with an X-ray Co radiation X-ray source (Co K α1 1.7901 Å and K α2 1.7929 Å, Detector: LynxEye). The instrument has a fixed divergence slit with an opening of 0.5° and 0.04 rad Soller slits. Reflections were measured between 5° and 90° 2 Theta (θ) with a step size of 0.02°. For Rietveld quantitative phase analysis (RQPA) 10 wt% silicon was added to the samples. Quantitative XRD samples were homogeneously mixed utilizing a McCrone micronizing mill (Retsch). Quantification was done with TOPAS 4.2 software from Bruker. All crystal structures for quantification were obtained from the ICSD

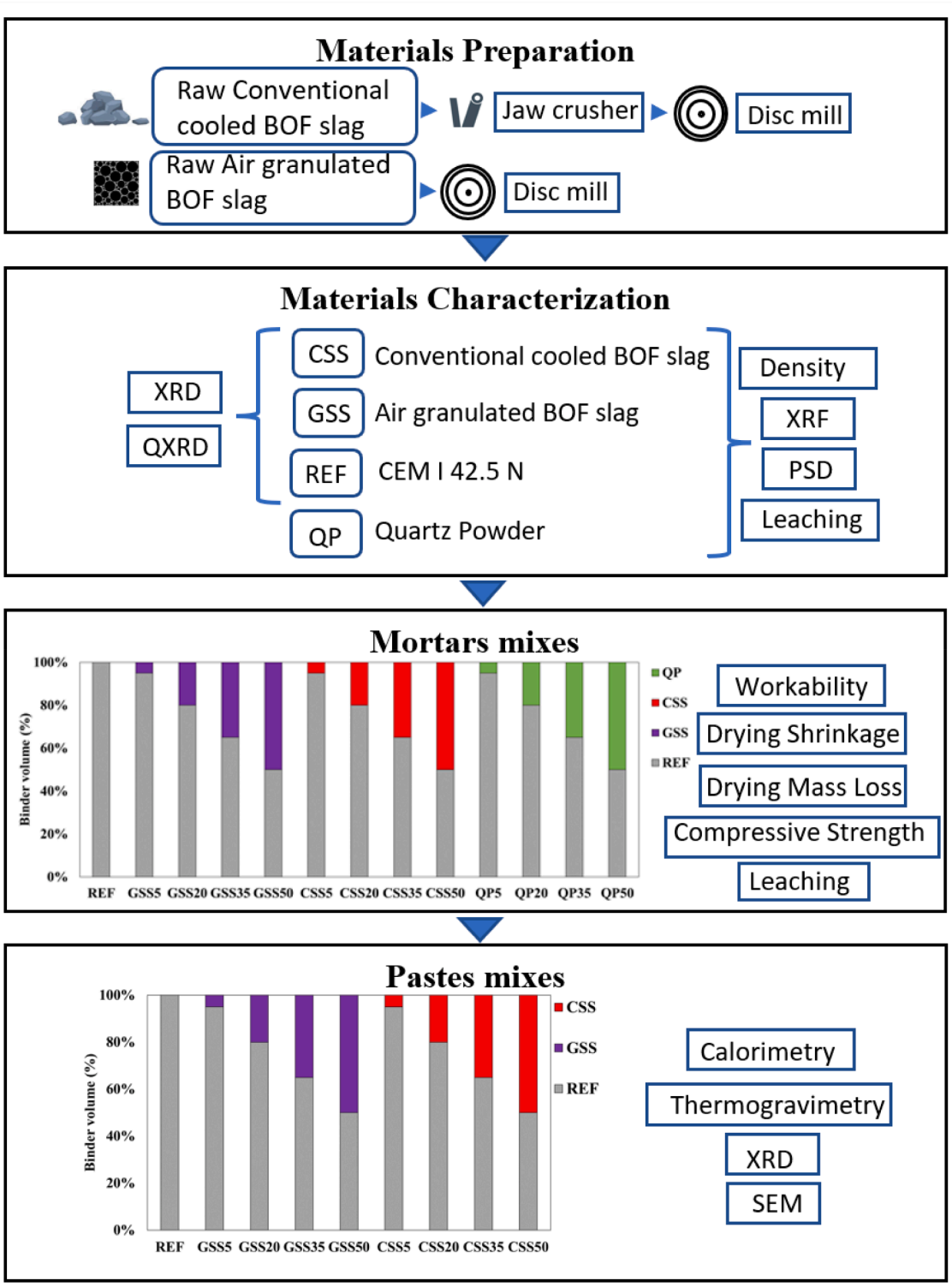

Fig. 1. Flow chart diagram for material preparation and characterization.

Table 1
The density of the material, sample label.

Material	Abbreviations	Density (g/cm^3)
CEM I 42.5N	REF	3.1
Quartz powder	QP	2.6
Conventional cooled BOF slag	CSS	3.6
Air granulated BOF slag	GSS	3.6

database. The peak assignment of the raw material is shown in Fig. 4 and a detailed quantitative analysis is presented in Table 3. (Please see Supplementary inf. Fig. S1(b, c) for Rietveld fit).

The mineral phases of all the raw materials have been presented in Table 3. The GSS and CSS exhibited almost the same mineralogical phases. The air granulation of the BOF slag leads to the formation of a high amount of α′-C_2S (22.0 wt%) as compared to the conventional cooled BOF slag (α′-C_2S = 7.8 wt%). Moreover, the iron-rich perovskite phase was observed only in GSS, which formed due to the breakdown of

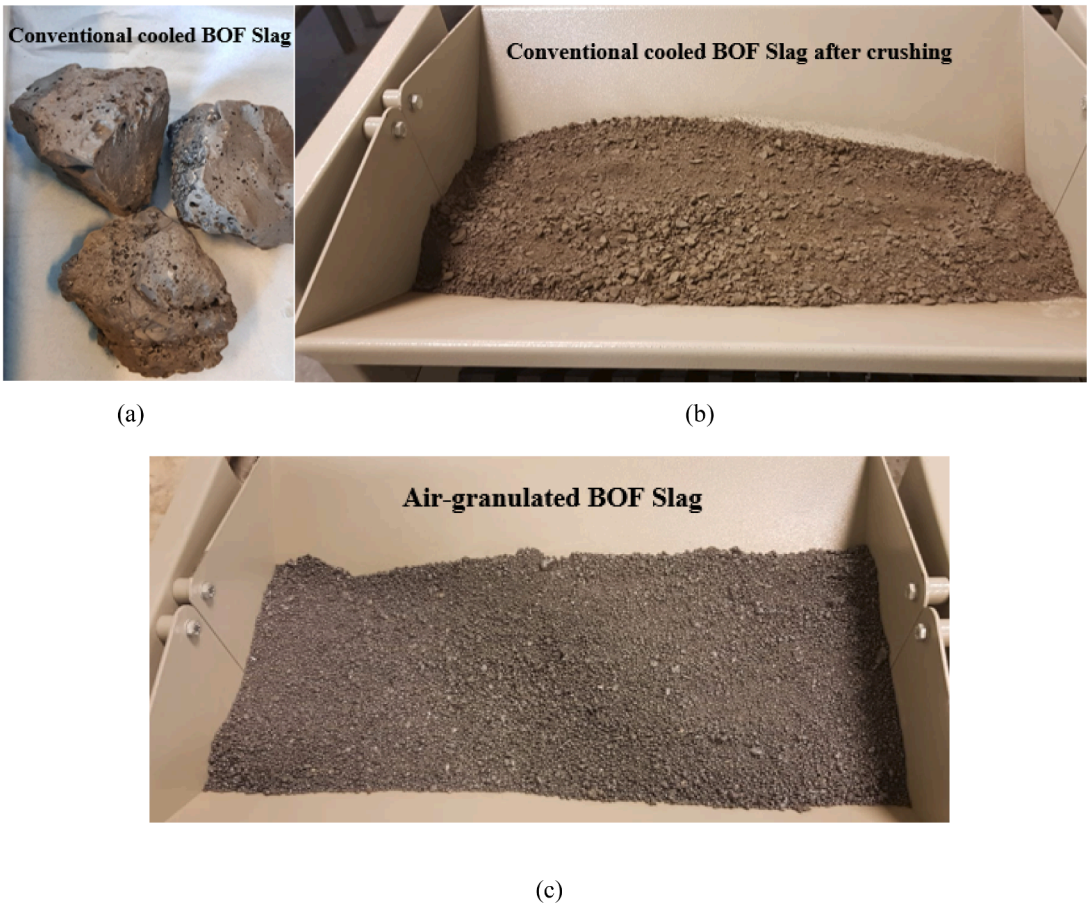

Fig. 2. The morphology of CSS fraction of (a) cobbles size (64–256 mm) and (b) reduced to sand size and (c) GSS, already received as sand size.

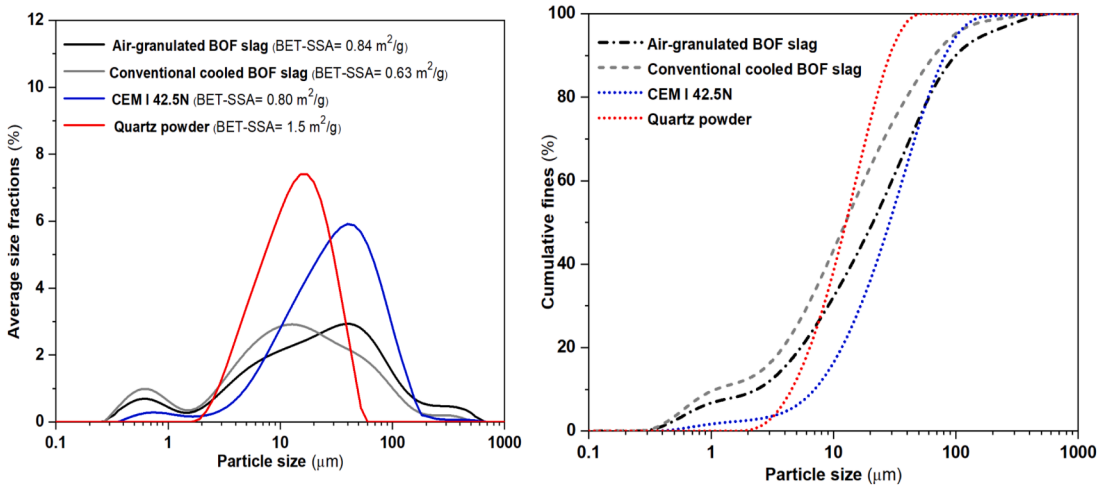

Fig. 3. The PSD (particle size distribution) of CEM I 42.5 N (SSA = 0.80 m^2/g), quartz powder (SSA = 1.5 m^2/g), air granulated BOF slag (SSA = 0.84 m^2/g) and conventional cooled BOF slag (SSA = 0.63 m^2/g) (a) average size fraction (%) (b) cumulative fine (%). The mentioned SSA (specific surface area) is obtained via the BET method.

brownmillerite due to quick cooling. A small amount of free lime (1.6 wt %) was observed in CSS while GSS exhibited no lime in the sample [39]. The CEM I sample contains a high amount of Hatrurite (tricalcium silicate ~60 wt%) which is responsible for the early age hydration activity of the cement [40]. The BOF slag sample contains a high amount of larnite + α'-C_2S (dicalcium silicate ~45 wt%) which highly contributes to the later age strength of the cement [41,42]. In this regard, the replacement of the cement with BOF slag could contribute to the synergy of chemical interactions.

Table 2
Oxide composition of GSS, CSS, CEM I, and QP in wt.%.

Material	MgO	Al_2O_3	SiO_2	P_2O_5	SO_3	CaO	TiO_2	V_2O_5	Cr_2O_3	MnO	Fe_2O_3	Others	LOI
GSS	7.3	1.3	12.5	1.2		44.6	1.3	0.7	0.3	3.9	26.8		−0.02
CSS	7.3	1.5	12.7	1.3		45.2	1.4	0.7	0.3	4.0	25.6		−0.1
CEM I 42.5N		4.2	17.7		3.1	64.6					3.3	3.2	3.9
QP		1.5	97.5								0.9		0.01

LOI = loss on ignition.

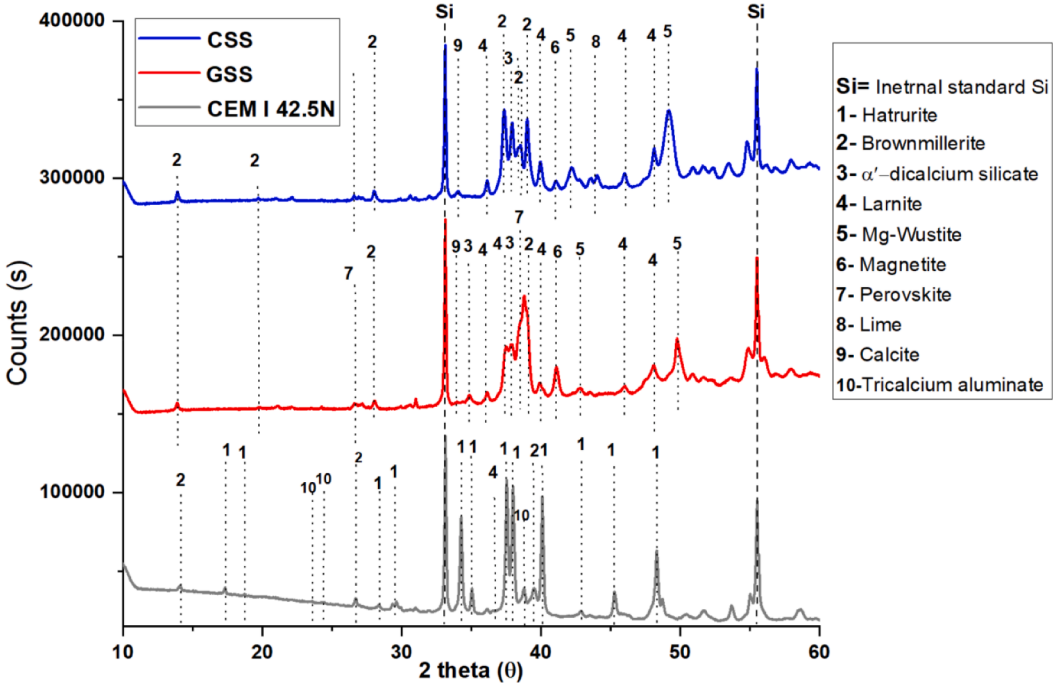

Fig. 4. X-ray diffraction (XRD) analysis of CEM I 42.5 N, GSS and CSS samples with labelled peaks.

Table 3
Quantitative X-ray diffraction (QXRD) of the CSS, GSS, CEM I 42.5 N in (wt.%).

Mineral Phases	Hatrurite	Larnite	α′-C_2S	Brownmillerite	Fe (Mg)-Wüstite + Magnetite	Perovskite	Lime	XRD amorphous	Others
CEM I 42.5N	59.6	5.71	2.11	11.6				14.1	6.7
GSS		16.9	22.0	25.7	17.6	6.4		10.1	1.3
CSS		33.2	7.8	22.0	29.2		1.6	5.5	0.7

Table 4
Mix design proportions of the mortars(vol.%).

MIX ID	CEM I 42.5N	CSS	GSS	QP	Standard Sand	Water/binder	OPC Replacement	Superplasticizer (% of total binder)
REF	0.22	0.00	–	–	0.78	1.2	0 %	0.25
CSS5	0.21	0.01	–	–	0.78	1.2	5 %	0.12
CSS20	0.17	0.04	–	–	0.78	1.2	20 %	0.12
CSS35	0.14	0.08	–	–	0.78	1.2	36 %	0.11
CSS50	0.11	0.11	–	–	0.78	1.2	51 %	0.12
GSS5	0.21	–	0.01	–	0.78	1.2	5 %	0.07
GSS20	0.17	–	0.04	–	0.78	1.2	20 %	0.07
GSS35	0.14	–	0.08	–	0.78	1.2	36 %	0.07
GSS50	0.11	–	0.11	–	0.78	1.2	51 %	0.07
QP5	0.21	–	–	0.01	0.78	1.2	5 %	0.10
QP20	0.17	–	–	0.04	0.78	1.2	20 %	0.10
QP35	0.14	–	–	0.08	0.78	1.2	36 %	0.10
QP50	0.11	–	–	0.11	0.78	1.2	51 %	0.13

Note: The mixes were designed from the starting REF by mass with Standard sand/binder = 3 and w/b = 0.4 kept constant for the design of all the other mixes in volume.

2.2. Mortars study

2.2.1. Mix design

For the mortars mix design, a reference (REF) of 100% of OPC (CEM I 42.5 N) was adopted and replacements of ~5, 20, 35, and 50% were done with GSS, CSS, and QP to evaluate the effect of replacing cement by GSS and to compare its performance concerning CSS and an inert material QP as shown in Table 4. The replacement percentages were chosen to start from 5%, to include in this study the possibility of using BOF slag as a minor additional constituent (MAC) as well.

The mixes were designed from a starting reference (REF) where the relation of standard sand/binder = 3 using a water/binder (w/b) ratio of 0.4 by mass. Those ratios were kept constant for the design of all the other mixes in volume. Samples were prepared according to EN 196-1 [43], composed of mass (25% of binder and 75% of standard sand). The value of w/b = 0.4 was chosen due to the reduced water demand of BOF slag. The fresh samples were cast in plastic moulds of 160 × 40 × 40 mm covered with a plastic film for the first 24 h, then demoulded and cured at a temperature of 20℃ until their testing age.

The REF was replaced with both (GSS and CSS) slags by volume from 0 to 50% with an amount of 5, 20, 35, and 50% and labelled as GSS/CSS-X (X = 5, 20, 35, 50). The quartz powder with the same degree of replacement as both slags was added to compare the material performance with inert material.

2.2.2. Fresh properties

Based on EN 1015–3:2004, a flow table was used to measure the fluidity of the fresh mortars. The w/s ratio was kept constant for all mixes and the flowability was adjusted with a superplasticizer (Sika ViscoFlow®-37 con. 32% SP-Polycarboxylate ether) to avoid discrepancies between the samples regarding workability. Afterwards, the fresh pastes were filled into the mould of 160 mm × 40 mm × 40 mm and vibrated for 60 s and covered with the plastic film for 24 h until further testing.

2.2.3. Mechanical properties

The compressive strength of the mixes was evaluated after 7, 14, 28, and 91 days. After casting, the specimen surface was covered with the film to prevent moisture loss and carbonation and placed at room temperature (21 ± 2 °C) for 24 h. The specimens were demoulded after curing for 24 h, and then specimens were kept for curing in standard curing conditions (21 ± 2 °C, 95 ± 3% relative humidity). The reproducibility of the result was evaluated from the average of at least three test results. The compressive strength of the specimens was measured at a speed of 2400 N/s.

2.2.4. Drying shrinkage

To determine the long-term properties, mortar specimens of 160 × 40 × 40 mm were prepared for the drying shrinkage test and the drying mass loss of the same prisms was measured according to DIN 52,450 [44]. The specimens were cured for 24 h at room temperature (21 ± 2 °C, 95 ± 3% RH), then taken to a room with 21 ± 2 °C and relative humidity of 60 ± 5% RH, where the drying shrinkage measurements were carried for 72 days when a further change in drying mass loss and shrinkage values become constant.

2.2.5. Leaching analysis

One batch leaching test was performed on raw material and 28 days mortar sample according to EN-12457 using deionized water with a liquid to solid ratio of 10. The mortar sample is crushed into a powder for good insight into the leaching behaviour of slag. The sample was placed in plastic bottles and shaken continuously for 24 h at 21 ± 2 °C. After the experiment, the liquids were filtered through a 0.2 μm Polyether sulfone membrane and stored at 5 °C after acidifying with nitric acid (65% supra pure) to prevent precipitation. Before acidification, the pH was measured. An ICP-OES spectrometer (Spectroblue FMX36) was used for quantitative analysis of the leachate. The leaching of raw material has been presented in Table 5. All the raw materials exhibited the leaching of heavy metals below the legal limits of the Dutch soil quality decree.

2.2.6. Pastes study

To understand the influence of reactivity on the mechanical properties, binder pastes with the same level of slag replacement with cement and water to binder ratio (w/b = 0.4) as used in mortar samples were mixed, sealed, and cured at room temperature until 7, 28, and 91 days.

2.2.7. Calorimetry

The early age hydraulic activity of the sample was analyzed with a TAM Air isothermal instrument at 25 °C. The samples were mixed with the water by hand for one minute before adding the sealed glass ampoules into the calorimeter.

2.2.8. Thermogravimetry analysis

The TG (thermogravimetry) analysis was performed on the hydrated paste samples via Jupiter STA 449 F1 (Netzsch) with heating of 15 °C/min under an N_2 environment up to 1000 °C.

3. Result and discussion

3.1. Physio-mechanical behaviour of cement-slag mortars

3.1.1. Workability

The spread flow values of the fresh mortars for each mix design are plotted in Fig. 5. The flowability of the REF was adjusted with 1.4 g of superplasticizer to achieve ~120 mm average diameter. The substitution of OPC by the BOF slags did not increase the fresh mortar diameter. In comparison to the spread-flow value of 120 mm presented by the REF mix, the values of GSS05, GSS20, GSS35, and GSS50 samples decreased to 107, 105, 100, and 100 mm respectively. The decreasing trend in fresh mixes in the present case can be attributed to a practical optimization point to avoid later bleeding and segregation. When compared to literature [45–47], the fresh mortars with replacements of slag presented a relative decrease in the spread flow value. The QP05 (100 cm), QP20 (100 cm), QP35 (100 cm), and QP50 (110 cm) also exhibited a relative decrease in fluidity due to a higher specific surface area (1.5 m^2/g) than REF (0.8 m^2/g). Usually, the higher fineness and specific surface area of QP than OPC increases the water demand of the mixture which leads to a decrease in flowability [48].

3.1.2. Mechanical performance

Compressive strength development of the mortar specimens tested at ages 7,14, 28, and 91 days is presented in Fig. 6(a, b, c, d). The 5% OPC replacement with BOF slag in GSS05 and CSS05 samples increased the 7-day compressive strength to ~63 and ~64 MPa, respectively. That is

Table 5
One batch leaching (NEN: 1245–7) analysis of raw materials.

Sample		CEM I 42.5N	Conventional cooled BOF Slag	Air granulated BOF Slag	Quartz Powder
*Element**	**pH Legal limit**	**13.1 mg/kg**	**12.3 mg/kg**	**12.4 mg/kg**	**9.8 mg/kg**
Sb	0.32	0.04	0.1	0.04	0.03
As	0.19	0.02	0.09	0.05	0.03
Ba	22	5.5	0.5	0.4	0.09
Cr	0.63	0.5	0.4	0.4	0.06
Mo	1	0.05	0.08	0.08	0.02
V	1.8	0.003	1.4	0.4	0.0
Zn	4.5	0.007	0.02	0.04	0.002
Fe		0.1	19.2	0.001	2.2

*Cu, Co, Hg, Ni, Se, Cd, Pb and Sn were below the detection limit.

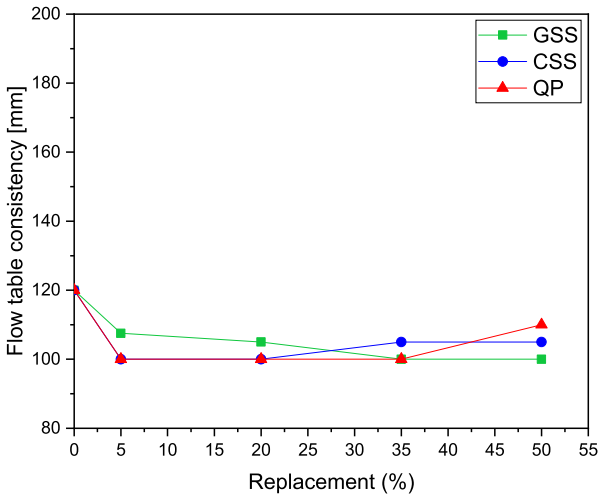

Fig. 5. Determination of consistence of fresh mortar by flow table (diameter) for REF and the replacements of 5, 20, 35 and, 50% of GSS, CSS and QP.

notably higher than the REF mix ~56 MPa mechanical performance [49,50]. At 28 days, the compressive strength of GSS05 reached ~70 MPa showing a significant increase compared to the REF mix of ~62 MPa, while CSS05 exhibited a decreasing trend in compressive strength performance. Upon further curing to 91 days, the CSS05 exhibited the highest compressive strength of ~74 MPa like the REF sample. Although, the GSS05 reached a plateau, and no further strength gain was observed during 28 to 91 days of the mortar. In comparison to the mechanical performance of the inert material (quartz powder), the 5% replacement cement-slag samples at all ages present a compressive strength considerably higher than QP05. After the 5% replacement, the compressive strength of all mixes starts decreasing with an inversely proportional relationship to the substitution in comparison with the reference mix. Moreover, the ~6–35% exhibited a mechanical performance analogous to inert material even having 44–58% lower specific surface area than quartz powder (Fig. 6(b, c, d) [21,34,51,52].

The slag samples with replacements up to 35% present compressive strength values higher than 42.5 MPa, which may not reach the REF values but exceed the strength requirements established by the standard (BS EN 197–1) (see activity index of mortar as compared to REF and QP in Fig. S2(a, b, c, d)). Although the BOF slag addition for GSS50 and CSS50 at all ages does not reach the REF and the standard requirements, both slag samples present comparable mechanical behaviour.

The continuous decrease in mechanical performance on higher than 5% slag substitution in OPC can be explained based on the cement-slag hydration because the cement-slag phases play an important role in the evolution of the mechanical performance of the mortar specimen [53].

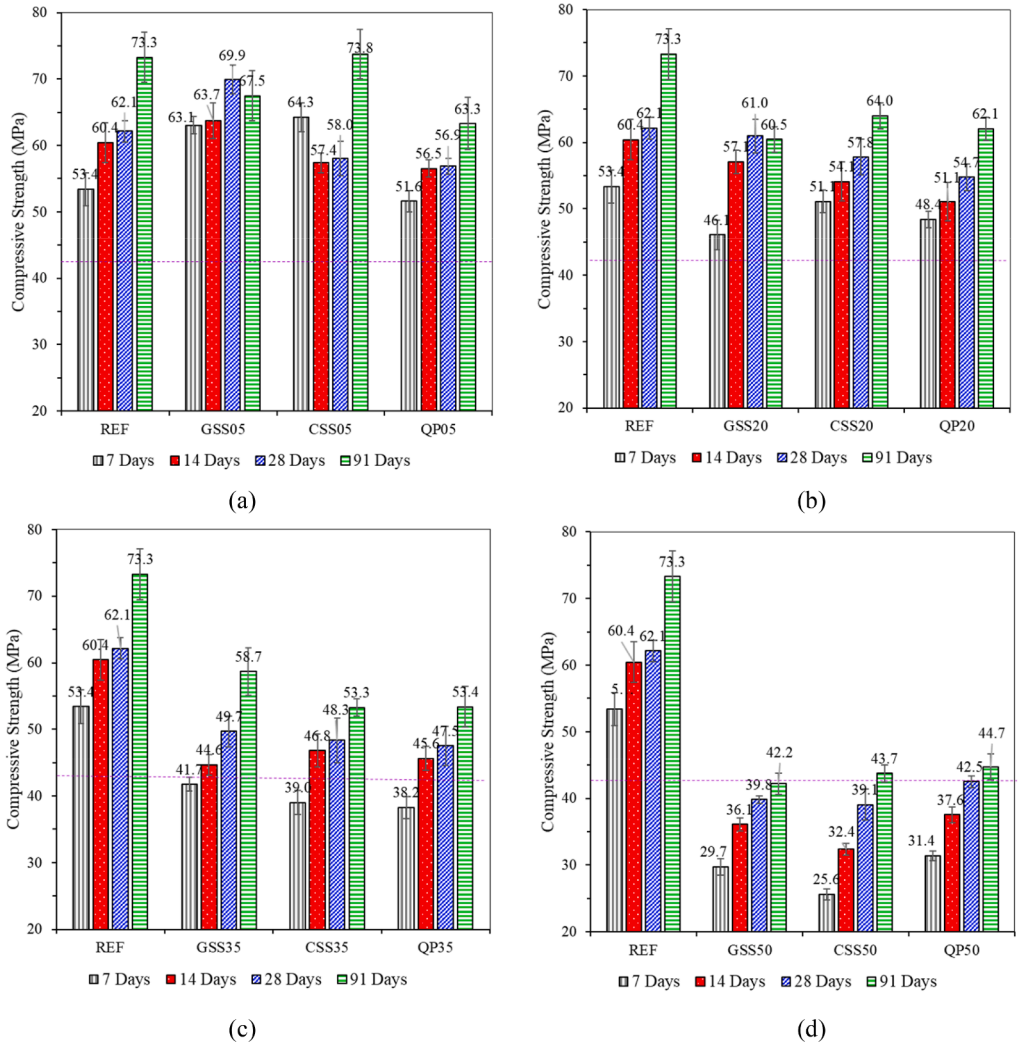

Fig. 6. Compressive strength of mortar specimen of 5, 20, 35 and, 50% of GSS, CSS and QP mixes (a) 5% (b) 20% (c) 35% (d) 50%. The dotted line refers to 42.5 MPa for means of comparison.

Therefore, a detailed hydration behaviour of slag substitution in OPC, and its correlation with mechanical behaviour is explained in section 3.2.

3.1.3. Drying shrinkage and drying mass loss

To understand the mechanical properties, the length stabilization of all the mortar specimens was measured till 72 days when reached constant values as shown in Fig. 7(a, c, e). Regardless of the mixture and replacement percentages, the length changes vary between 0 and 1 mm/m, and observed values were close to the REF. The highest drying shrinkage value of 0.99 mm/m for CSS50 was observed at 23 days of curing and posing no harm to the volume stability of mortars [54]. In general, most mortar specimens reached their 95% drying shrinkage by 28 days. Moreover, the GSS05, CSS05, GSS20, and CSS20 exhibited high length stabilization after 37 days as well as the REF mortar specimen.

For further validation of BOF slag mortar stability, the drying mass

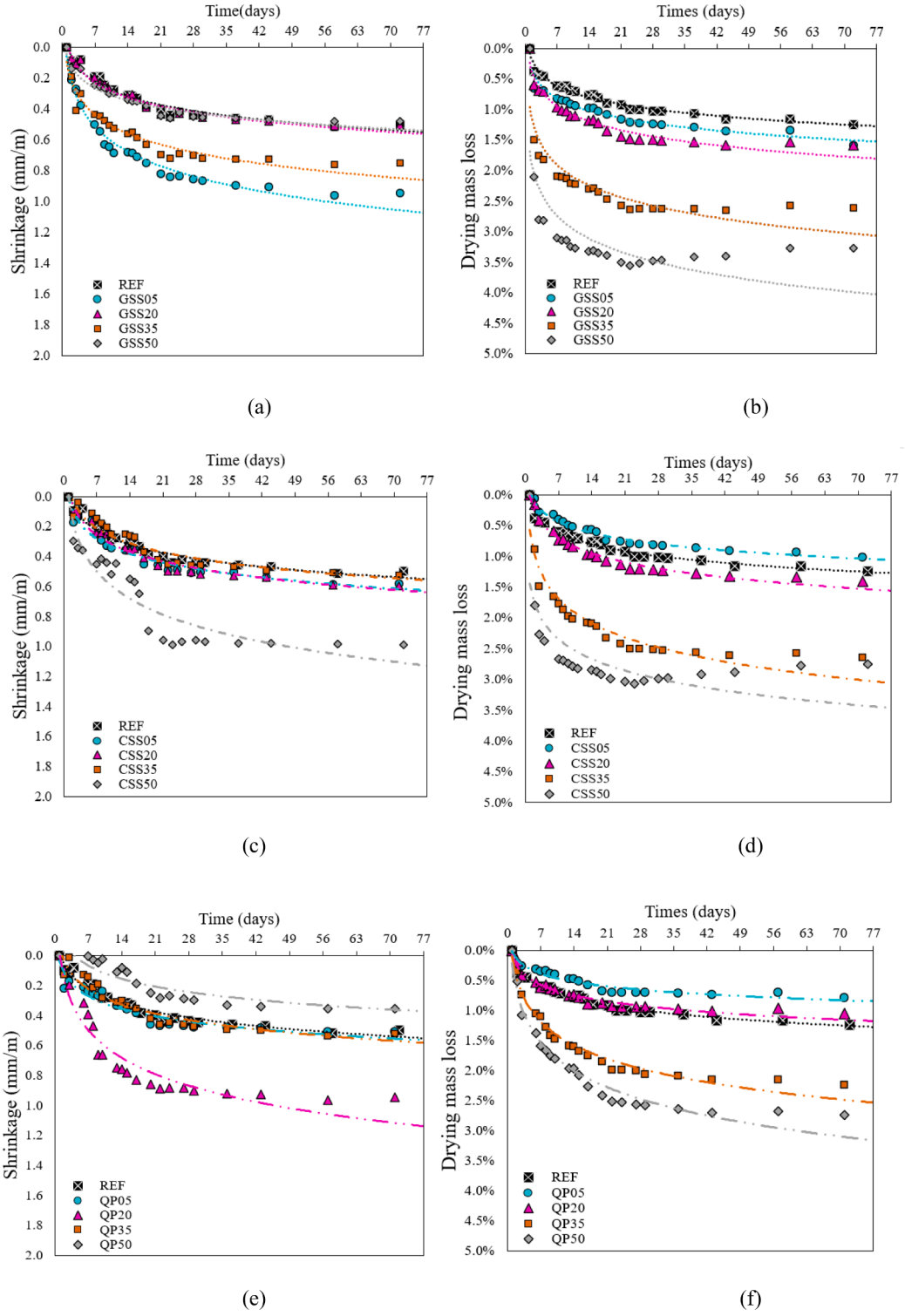

Fig. 7. Drying shrinkage of mortar specimens of 5, 20, 35 and, 50% replacement by (a) GSS, (c) CSS and (e) QP in comparison to the REF sample. Mass change of mortar specimens of 5, 20, 35 and, 50% replacement by (b) GSS, (d) CSS and (f) QP, in comparison to the REF sample.

stability of the mortar sample was measured over 72 days as shown in Fig. 7(b, d, f). The percentage drying mass loss varies between 0 and 4.0% in the replacements of GSS, especially the GSS50, the sample that reaches the highest drying mass loss (3.56%) after 23 days of curing. Among the 3 different materials used for replacements, those with the highest percentages of substitution (35 and 50%) reach their highest drying mass loss value at 23 days. A clear correlation exists between the replacement of OPC with BOF slag and drying mass loss might correspond to the slow reaction of the BOF slag phase's reaction with OPC leading to more available capillary water for evaporation. The GSS05, CSS05, GSS20, and CSS20 specimens exhibited a drying mass loss $\leq$1% and the values are closer to the REF sample, correlating well with the compressive strength values.

The physio-mechanical properties of cement-slag mortar exhibited the air granulated BOF slag fitness as a binder. But as the amount of BOF slag increased from 5 to 20%, the compressive strength of GSS20 and CSS20 significantly decreases in comparison to the REF mortar specimen. The early and later stage reactivity of cement (hatrurite, calcium aluminoferrite phases) and BOF (larnite, brownmillerite) slag phases contributes significantly toward the evolution of strength development [52]. To understand the correlation between cement-slag reactivity and mechanical performance, the cement-slag pastes hydration is investigated over time as presented in section 3.2.

3.2. Reactivity of pastes and its correlation with mechanical performance

3.2.1. Early age hydration studies

The early age hydration behaviour of cement-slag paste has been investigated via isothermal calorimetry as shown in Fig. 8. The exothermic heat of hydration is normalized with the mass of the sample. The early age (48–72 h) reactivity is dependent on the specific surface area (SSA). The SSA among the samples REF (0.80 m^2/g) and GSS (0.84 m^2/g) are comparable, while the sample CSS (0.63 m^2/g) contains 21% lesser SSA than the REF (Fig. 3) [55]. So, the early-stage (0–72 h) reaction between air granulated BOF slag and CEM I is directly comparable. A typical hydration process of OPC is comprised of five stages such as rapid heat release period, dormant period, acceleration period, deceleration period, and steady period respectively which can be observed in the REF sample as shown in Fig. 8(a, b) [56].

The first exothermic peak in 1–2 h can be attributed to the partial dissolution of the cement. Therefore, the cement hydration enters the dormant period after the first exothermic peak of dissolution [57]. The second exothermic peak around 3–7 h can be attributed to the reactivity of the calcium aluminate (AFm) phases [46,58]. As the hydration products such as C—S—H and $Ca(OH)_2$ precipitate only when the concentration of Ca^{2+} in the solution reaches a saturation state [59]. The apex point of the exothermic peak appears around ~18 h and is caused

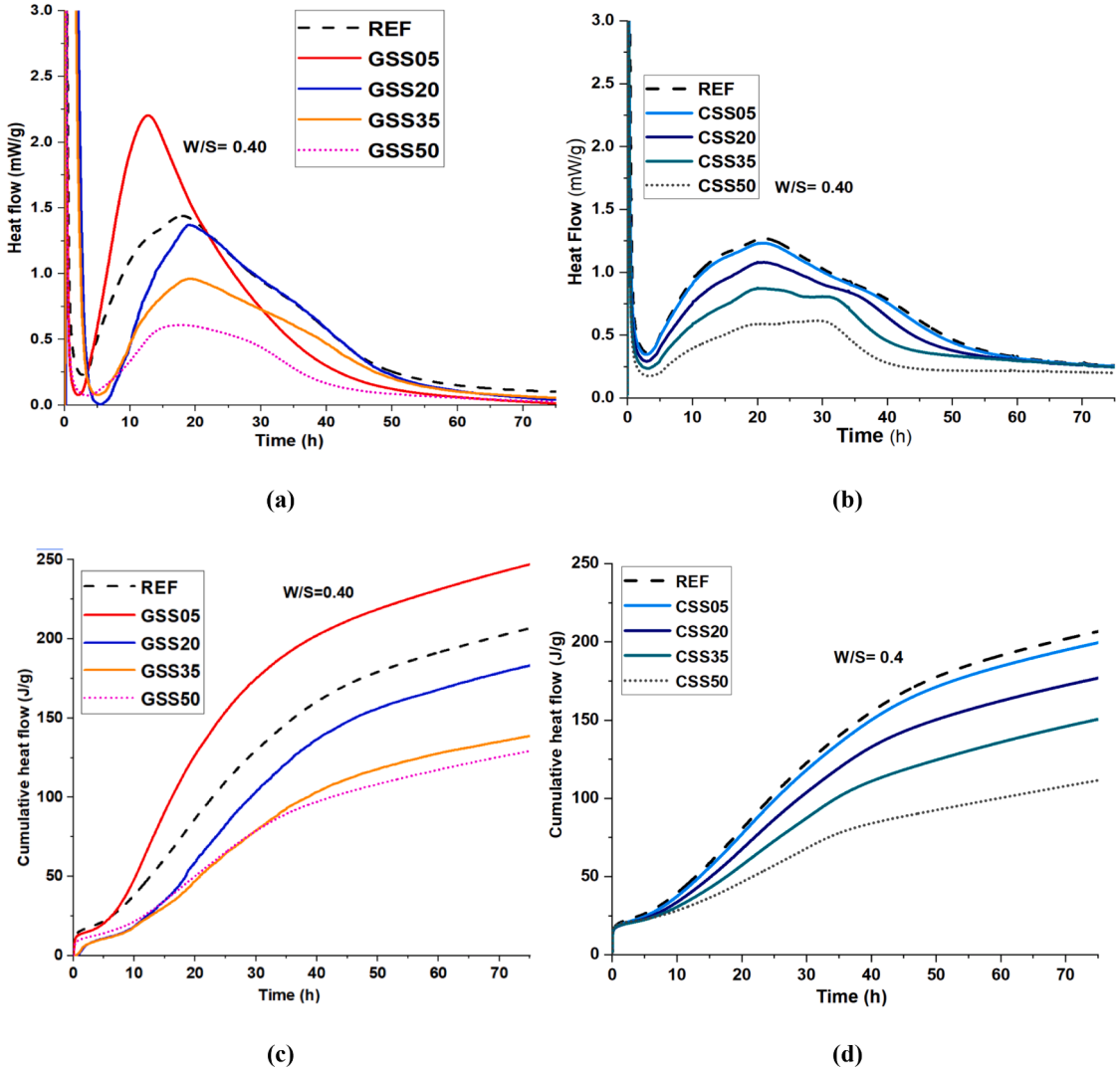

Fig. 8. The exothermic heat curve of cement-slag with reference to cement (a) heat flow of Cement-GSS clusters (b) heat flow of Cement-CSS clusters (c) cumulative heat flow of cement-GSS clusters (d) cumulative heat flow of cement-CSS clusters.

due to precipitation of C—S—H (calcium silicate hydrate) and CH (portlandite). Then, the deacceleration heat flux persists for ~20–40 h which is consistent with the previous literature [34,60]. The 5% replacement of cement with the air granulated slag decreases the early dormant period, and the precipitation of C—S—H phases occurred earlier ~13 h indicating the clear synergy between the slag and cement in the GSS05 sample. In addition to that, the cumulative heat release of the GSS05 sample reaches ~246 J/g as compared to the CEM I sample at ~207 J/g (Fig. 8(c)). A further increase in cement replacement with the air granulated slag in GSS20, GSS35, and GSS50 samples decreases the rate of hydration incrementally than in the REF sample which indicates that the hydration is primarily dominated by the hatrurite (Ca_3SiO_5-alite) reactivity. The hydration degree of the conventional cooled BOF slag with 5% substitution in the CSS05 sample did not show any increase or decrease in the early-stage reactivity as compared to the CEM I sample (Fig. 8(b, d). It can be attributed to the lesser SSA (0.63 m^2/g) available for CSS reactivity than GSS. At higher replacement than 5% in CSS20, CSS35, and CSS50, an incremental decrease is observed in early-stage heat of hydration upon increasing the slag amount in cement-slag paste just like air granulated BOF cement-slag paste. A clear decrease in the reactivity of cement-slag paste is observed upon the addition of >5% CSS in the cement-slag paste.

For a better understanding of the enrichment of cement phases with the slag and mineral phase's reaction at an early age, a ternary composition diagram has been presented in Fig. 9. To make the composition diagram, the value of the mineral composition is taken from the QXRD of the raw material and normalized to 100% (Table 3). It indicated that the addition of 5% slag in cement does not alter the composition of cement significantly. But 20, 35, and 50% substitution of the cement with slag enriches the cement-slag composite with brownmillerite, dicalcium silicate and RO (Mg-wüstite phases) while decreasing the amount of hatrurite. As it is concluded that the early-stage (48–72 h) hydration of the cement-slag composite is dominated by the reaction of tricalcium silicate (Fig. 8). The composition diagram pointed out that the replacement of cement with slag leads to a new composition. The new phase composition would enhance the chances of a decrease in reactivity due to the enrichment of slow-reacting phases such as dicalcium silicate, Fe, Mg-wüstite and decreasing amount of hatrurite. The possible hydration synergy between cement and BOF slag at an early age can only be achieved if the brownmillerite would significantly contribute to the hydration reaction alongside the hatrurite phase. Unfortunately, that is not the case with the BOF slag substitution in cement as shown in Fig. 8. A few studies explained the slag retardation effect on the early age hydration of cement which has been attributed to low alkali content, slow depletion of gypsum and reduction in the formation of ettringite [34,61]. But the ternary composition diagram provides a new perspective to understand the possible slag activation

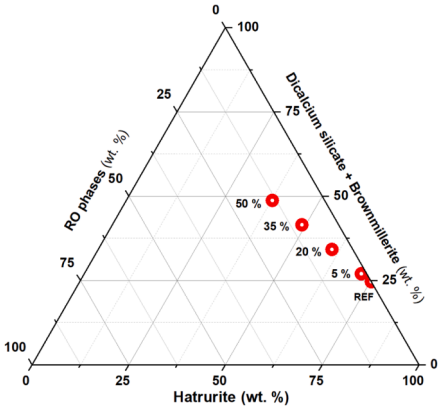

Fig. 9. The mineralogical composition of the cement-slag composite changing with the increase of cement replacement by BOF slag.

efforts as a cementitious binder. Moreover, the hydration of brownmillerite is highly dependent on the Al/Fe ratio in the solid solution and the amount of added sulfate alongside the presence of possible minor ions [62,63]. Without this knowledge, the cement-slag composite reactivity at solution level cannot be well explained.

3.2.2. *Characterization of hydration products*

Differential thermogravimetric analysis (DTG) was used to determine the dominant hydration phases. The curves for the cement-slag pastes after 7, 28, and 90 days are shown in Fig. 10(a, b, c, d, e, f (thermal mass loss events can be found in Fig. S3). The mass loss events have revealed that GSS05, CSS05, and REF samples exhibited higher mass loss at 40–200 °C (dehydration of calcium silicate hydrate and ettringite, AFm), 340–400 °C (dehydration of double layer hydrotalcite), 430–510 °C (dehydration of calcium hydroxide), and 550–800 °C (decarbonation of calcium carbonate) than GSS (20–50%) as well as CSS (20–50%) cement-slag paste [64]. The mass loss events indicated that the cement-slag paste hydration reaction is dominated by the hydration of tricalcium silicate and dicalcium silicate. The assigned mass loss events in the thermal analysis of cement-slag paste are further confirmed by analyzing the X-ray diffraction pattern of 90 days of cured cement-slag paste of both slags as shown in Fig. 11(a, b). The crystalline hydration phases such as ettringite, tetra calcium aluminate monocarbonate hydrate (C_4A-monocarbonate hydrate) as well as hydration products of C_3S and C_2S such as calcium silicate hydrate, portlandite and calcite (formed upon carbonation of portlandite) was observed. Moreover, a double-layer hydrotalcite, especially pyroaurite and Zn-rich hydrotalcite, was observed in the 90 days of hydrated air granulated and conventional cooled cement-slag paste composite. The type of hydration products is further complemented by microstructure analysis of 28 days cured past sample as shown in Fig. 12. The SEM-BS (back-scattered images) of 28 days cured 100% cement sample exhibited the well intercalated hydration phases of C—S—H, ettringite, portlandite and calcite (Fig. 12(a, b)) [20,65]. The addition of 5% BOF slag substitution in cement exhibited dense hydration that was significantly distributed all over cement-slag composite grains (Fig. 12(c, d)). Upon 50% slag replacement, a clear decrease in homogenous hydration products distribution with unreacted slag particles is observed in the cement-slag composite (Fig. 12(e, f)).

The bound water due to cement-slag hydration decreases incrementally upon the incremental replacement of cement with the slag as compressive strength drops in the mortar sample (Fig. 5). Moreover, the cement-slag composite lacks brownmillerite reactivity even till 90 days of curing (Figs. 10, 11). The observation is further confirmed due to the lack of mass loss event at ~260–390 °C usually attributed to Fe-siliceous hydrogarnet formation upon the reactivity of brownmillerite. A typical hydrated BOF steel slag usually contains Fe-siliceous hydrogarnet (hydroandradite) and Fe-katoite alongside calcium silicate hydrate due to brownmillerite hydration [66]. Because the formation of Al-siliceous hydrogarnet (hydrogrossular) is hindered kinetically at room temperature [67]. The formation of hydrogarnets is usually restricted under a cementitious system. In addition to that, a significant amount of up to 50% aluminium in hydrated slag blended-cement is incorporated in C-A—S—H while uptake of Fe (III) is negligible as compared to aluminium [62,67,68]. All these factors can contribute to inhibit the brownmillerite reaction.

By juxtaposing the early-stage hydration as well as the cement-slag composition diagram (Figs. 8, 9), the microstructure as well as diffraction pattern of hydration products and DTG analysis of cement-slag paste cured for 7, 28, and 90 days (Figs. 10, 11, 12), it is concluded that the enrichment of cement with slag phases inhibits the reactivity of the BOF slag brownmillerite and restricts the formation of Fe-siliceous hydrogarnet till 90 days. Moreover, the GSS and CSS contain dicalcium silicate alongside brownmillerite that usually reacts slowly till 28 days leading to a delay in cement-slag reactivity at a higher replacement than 5% [42].

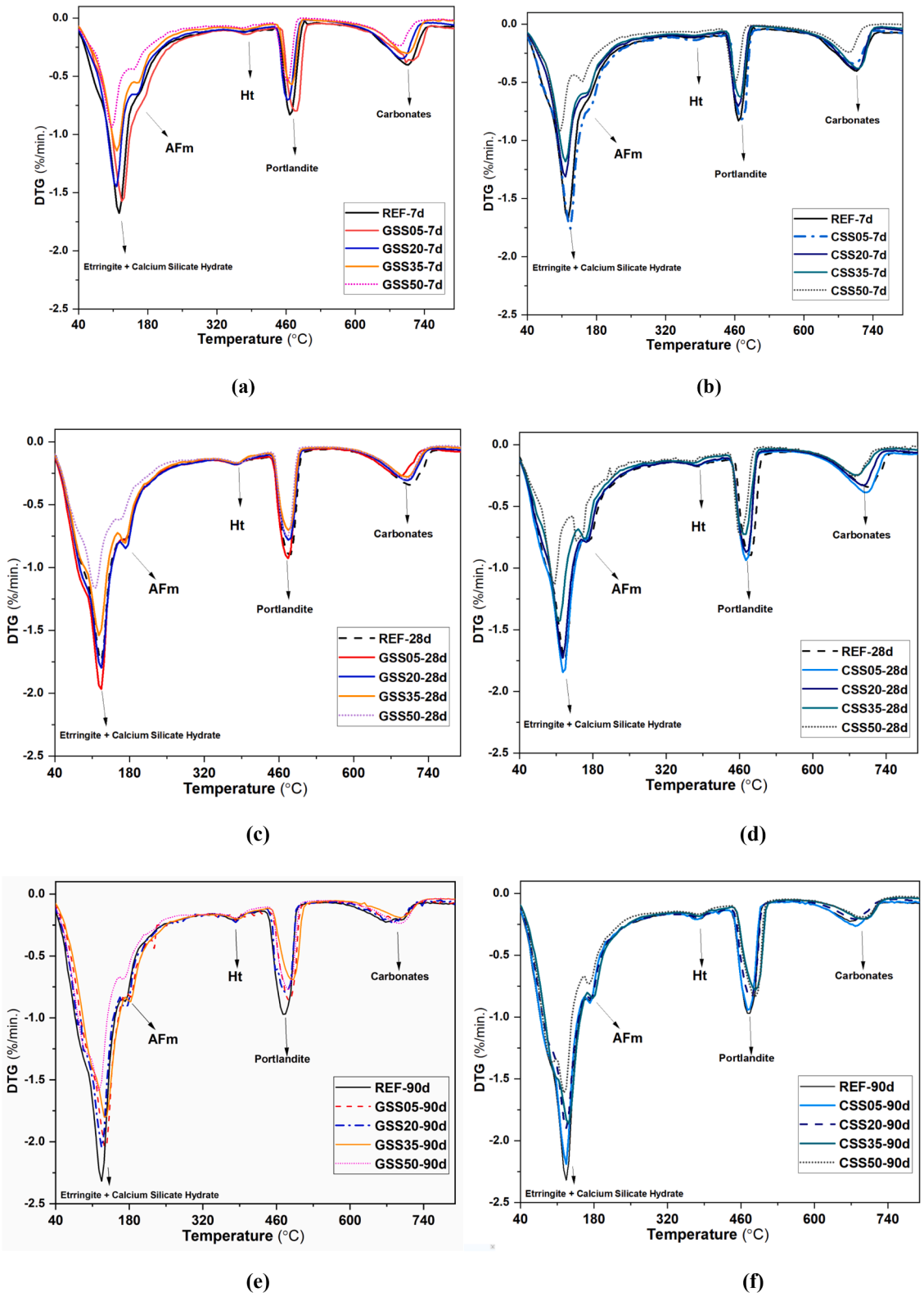

Fig. 10. DTG analysis of cement-slag pastes sample with 5, 20, 35 and 50% replacement of cement with BOF slag in comparison of REF, cured for (a) GSS-7 days (b) CSS-7 days (c) GSS-28 days (d) CSS-28 days (e) GSS-90 days (f) CSS-90 days. The mass loss event is assigned as ettringite + calcium silicate hydrate, AFm (C_4A-C hydrate), Ht (hydrotalcite), Portlandite (calcium hydroxide), and calcite (calcium carbonate).

3.2.3. Correlation of bound water with mechanical performance

Considering the importance of cement-slag reactivity on strength development in mortar, chemical-bound water is calculated from cement-slag paste samples and plotted against the mortar compressive strength as shown in Fig. 13. Even having the two independent studies (mortar and paste), the compressive strength of all the mortar replacement clusters is directly proportional to the chemical-bound water of the cement-slag paste which indicates the importance of cement-slag

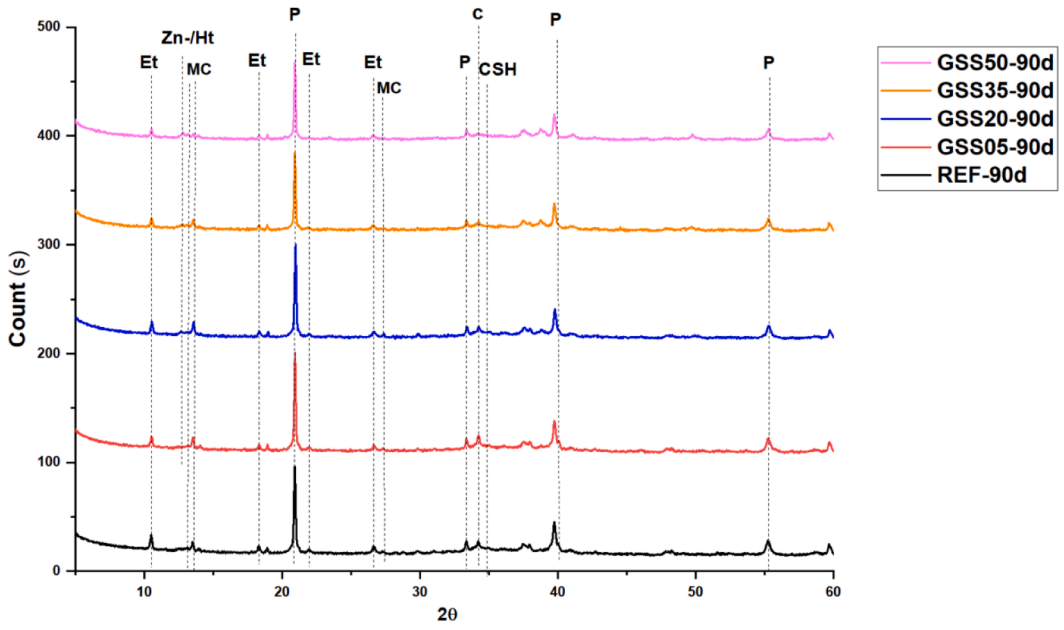

(a)

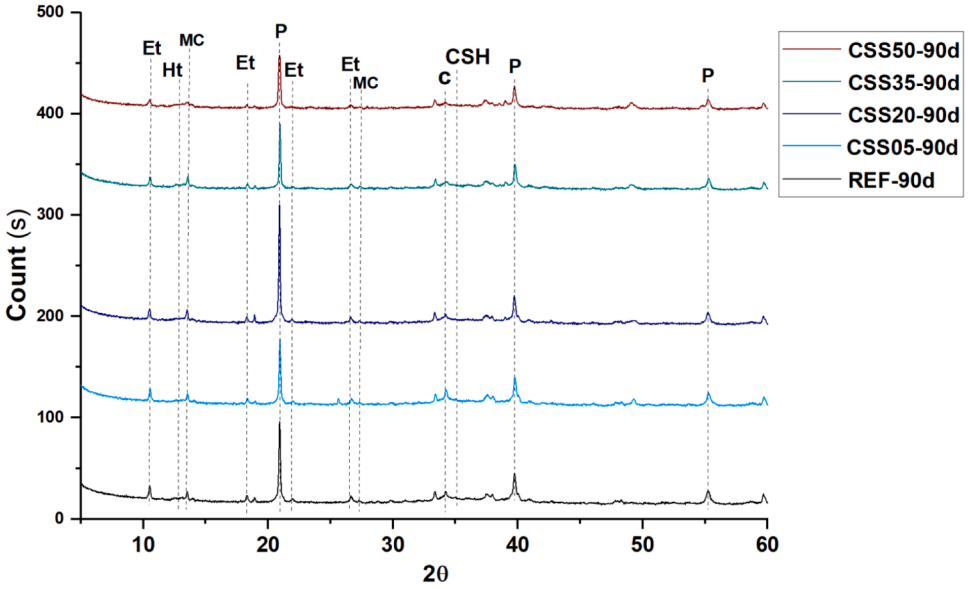

(b)

Fig. 11. XRD analysis of 91 days cured paste sample **a)** REF, GSS (05, 20, 35, 50) **b)** REF, CSS (05, 20, 35, 50). The peak of hydration products is labelled as Et = ettringite, MC = C_4A-monocarbonate hydrate, Ht = hydrotalcite, Zn-/Ht = Zn-hydrotalcite, P = Portlandite, C = calcite.

reactivity for mixed design applications. Comparing the conventional cooled and air granulated slag, overall, the GSS (5–50%) samples exhibited slightly higher chemically bound water (hydration degree) as compared to the CSS (5, 20, 35, 50). The value of bound water in GSS05 increases from ~20 to 21% between 28 and 90 days respectively which explains the insignificant change of mortar strength from 28 to 91 days. While CSS05 cement-slag paste bound water increases from ~18 to 21% between 28 and 90 days which interprets a higher increase in mortar strength from 28 to 91 days. Overall, no significant differences in mechanical performance, as well as hydration activity of the air granulated and conventional cooled BOF slag are observed except the former reacts faster than the latter one. In addition to that, the air granulation BOF slag can save grinding costs and improve the grindability of BOF steel slag. An extra grinding step of material crushing could be avoided before grinding in the case of conventional cooled BOF slag as reported above.

3.3. Environmental impact

One batch leaching test was performed on the 28 days cured mortar sample as shown in Table 6 (see Table S1 for QP (5–50%) mortar specimen leaching). All raw material exhibits heavy metal leaching below the permissible limits (Table 5). The replacement of cement with BOF slag decreases the V leaching significantly as compared to raw material (0.4 and 1.4 mg/kg for GSS, CSS respectively). While the Cr leaching increases in the GSS sample. The $Ca_3(VO_4)_2$ and $CaCrO_4$ are the dominant chemical species at pH >12. Usually, calcium vanadate is insoluble, and calcium chromate is soluble >20 g/L at room temperature which indicates that Cr is immobilized by the hydration products

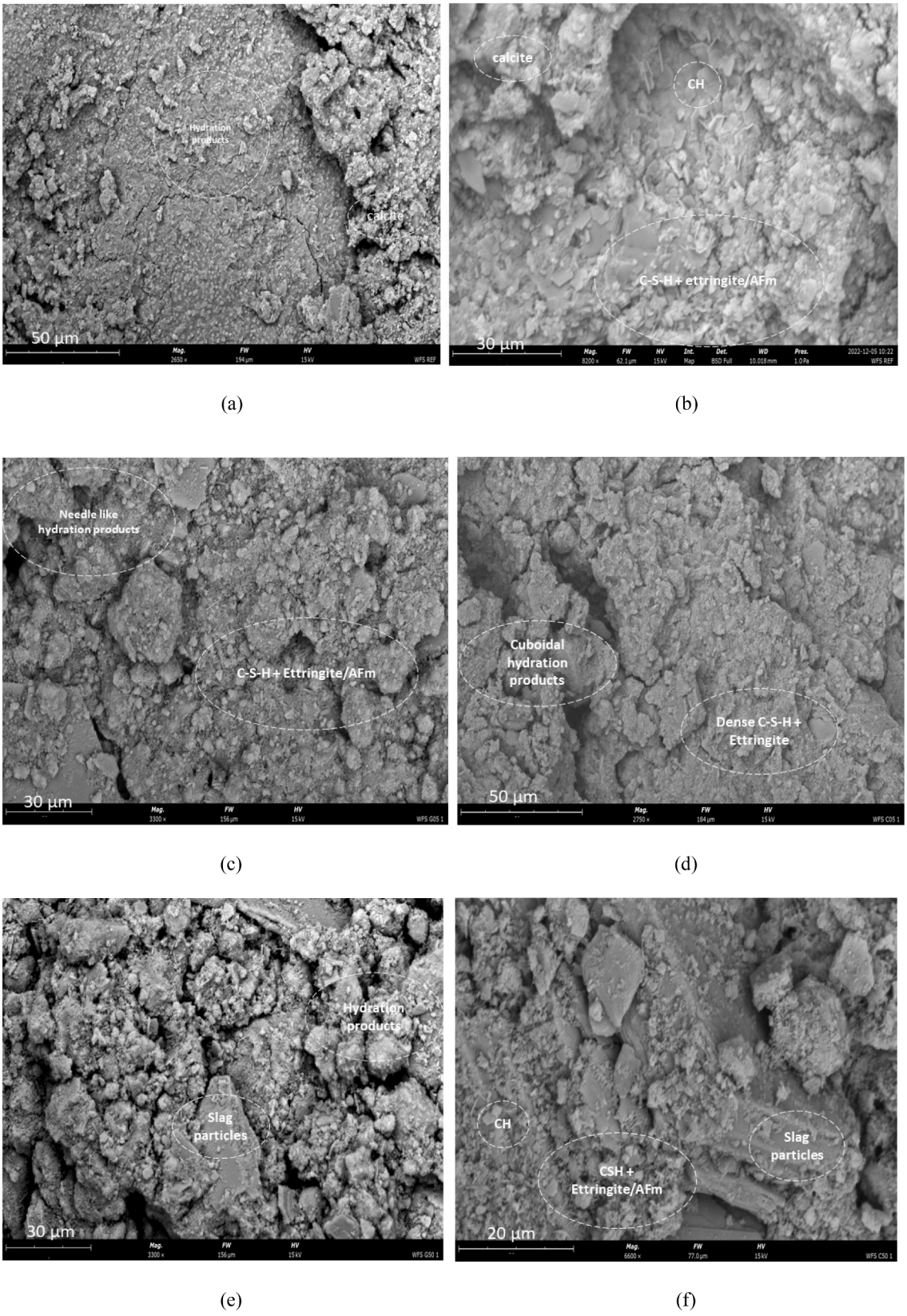

Fig. 12. SEM analysis of 28 days cured cement-slag paste **(a)** REF (50 µm) sample **(b)** REF (30 µm) sample **(c)** GSS05 (30 µm) **(d)** CSS05 (50 µm) **(e)** GSS50 (30 µm) **(f)** CSS50 (20 µm).

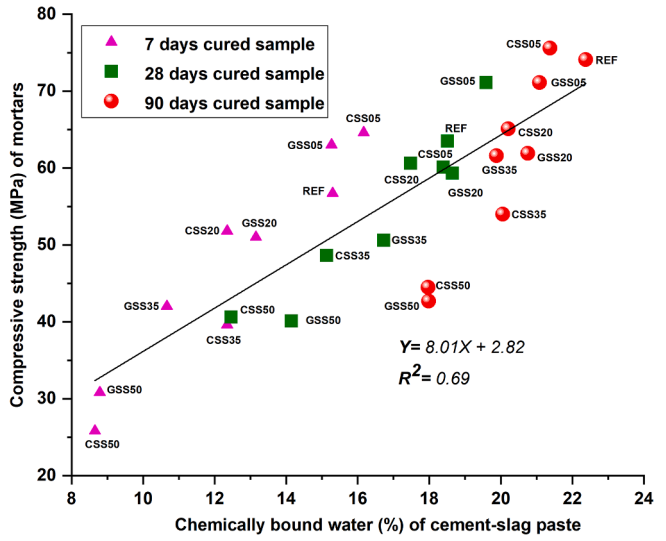

Fig. 13. The correlation between the chemically bound water of cement-slag pastes and the strength development of mortar samples cured for 7, 28, and 90 days.

[69,70]. Moreover, the barium leaching increases in mortar samples as compared to raw material (5.5 mg/kg CEM I). Usually, BOF slag exhibits the problem of heavy metal leaching particularly V and Cr [71,72]. Moreover, ordinary Portland cement also contains leachable chromium oxide [73]. The leaching of aliovalent heavy metals (V and Cr) is highly dependent on the oxidation state. In BOF slag, V exhibits V (III, IV, V) oxidation state while Cr is present as (II, III) as well as in cement. But it is established that the leached Cr and V contain the potentially hazardous oxidation state (VI) and (V) respectively [74,75]. Overall, the leaching values exhibited that the BOF slag is a suitable candidate to mix with OPC.

4. Conclusion

The study aimed to demonstrate that air granulation of BOF steel slag can be considered a viable solution for slag valorisation as binder as well as filler replacement in mortar application. For this purpose, cement is replaced by 5–50% clusters of air granulated as well as conventional cooled BOF slag and compared to inert material (quartz powder). Moreover, a detailed study of the cement-slag pastes is investigated to understand the correlation between the cement-slag reactivity and the mechanical performance of the novel binder. The main conclusions are as follows:

- Air granulated and conventional cooled BOF slag having a 5% replacement in OPC exhibited higher compressive strength than the reference and greater than quartz powder as well. While the substitutions of 20% and 35% of BOF slag are like the quartz powder.
- All 28 days cured cement-slag mortar samples exhibited the Cr and vanadium leaching below permissible limit according to the Dutch soil quality decree. Overall, 5% slag can be substituted in OPC as a binder and ~6–35% as an inert filler.
- The addition of the slag does not affect the mortars' stability, since the length variations were below 1 mm/m. All samples replacing 5 and 20% do not show considerably higher drying mass loss in comparison with the REF. In replacements of 35 and 50%, not only slags but quartz powder also, show a higher percentage of the mortars drying mass loss ~2–3.5%, an effect of the capillary water evaporation. The high drying mass loss in 35 and 50% clusters indicated that the water to solid can be lowered to get better mechanical performance.
- Cement-slag composite study revealed that the degree of hydration is crucial to understand the mechanical performance of novel binder. The enrichment of the cement with the 5% air granulated BOF slag increases the early-stage hydration reaction by lowering the Ca^{2+} saturation time from ~18 to 13 h in the early stage (0–72 h). The incremental addition of more than the 5% slag cement delays the hydration reaction of hatrurite at early stage. At later stages (1–90 days), the decrease in reactivity can be attributed to the absence of brownmillerite reactivity in a cementitious environment inhibiting the formation of Fe-containing siliceous hydrogarnet. A correlation between the strength development of cement-slag mortar and chemical bound water calculated from cement-slag pastes indicated that the compressive strength development is directly proportional to the degree of cement-slag reactivity at different ages.
- Air granulated BOF slag exhibited better hydration activity and mechanical performance than conventional cooled slag for up to 28 days. Overall, the air granulation of BOF slag did not affect the cement-slag composite performance significantly till 90 days. Moreover, the air granulated slag exhibited a good grindability that can reduce the cost of energy-intensive grinding steps of jaw crushing which can enhance the economic viability of BOF recycling.

5. Outlook

In summary, current study provides comprehensive understanding about air granulated BOF slag potential as binder and filler in building material application. This study shows that the air granulation shows the promise of grindability, workability, volume stability, better early age mechanical performance and environmentally safe building product. This knowledge can be used to valorize BOF slag by mechano-chemical, alkaline activation, partial replacement with industrial by-products. The air granulation as a step for the slag valorization was the main aim of this study.

CRediT authorship contribution statement

M. Jawad Ahmed: Conceptualization, Investigation, Methodology, Validation, Writing – original draft, Writing – review & editing. **Winnie Franco Santos:** Conceptualization, Investigation, Methodology,

Table 6
One batch leaching (NEN: 1245–7) analysis of 28 days cured mortar sample.

Sample		REF	GSS50	GSS35	GSS20	GSS05	CSS50	CSS35	CSS20	CSS05
pH		**12.9**	**12.3**	**12.6**	**12.7**	**12.9**	**12.5**	**12.7**	**12.7**	**13**
Element*	**Legal limit**	**mg/kg**	**mg/kg**	**mg/kg**	**mg/kg**	**mg/kg**	**mg/kg**	**mg/kg**	**mg/kg**	**mg/kg**
Si		0.17	0.01	0.01	0.02	0.02	0.02	0.02	0.02	0.02
Al		0.14	0.03	0.03	0.01	0.01	0.03	0.03	0.03	0.03
Ba	22	10.3	10.2	11.4	9.2	11.8	9.2	11.5	11.8	12.3
Cr	0.63	0.2	0.5	0.3	0.2	0.19	0.05	0.03	0.05	0.3
Mo	1	0.05	0.07	0.06	0.02	0.01	0.03	0.03	0.03	0.03
V	1.8	0.002	0.001	0	0.001	0.001	0.002	0.002	0.003	0.003
Zn	4.5	0.004	0.03	0.02	0.03	0.02	0.03	0.04	0.04	0.04

*Fe, Sb, As, Cu, Co, Hg, Ni, Se, Cd, Pb and Sn were below the detection limit.

Validation, Writing – original draft, Writing – review & editing. **H.J.H. Brouwers:** Project administration, Resources, Supervision, Visualization, Writing – review & editing.

Declaration of Competing Interest

The authors declare that they have no known competing financial interests or personal relationships that could have appeared to influence the work reported in this paper.

Data availability

Data will be made available on request.

Acknowledgment

The authors would like to acknowledge the financial support from NWO (The Netherlands Organisation for Scientific Research) for funding this research (project no.10023338) and M2i (Materials Innovation Institute, project no. S81.6.15565b) for managing this project. Furthermore, the authors wish to express their gratitude to the following sponsors of this research: Tata Steel; ENCI; V.d. Bosch Beton; Blue phoenix group; Hess.

Appendix A. Supplementary data

Supplementary data to this article can be found online at https://doi.org/10.1016/j.conbuildmat.2023.130342.

References

[1] W. Shen, L. Cao, Q. Li, W. Zhang, G. Wang, C. Li, Quantifying CO_2 emissions from China's cement industry, Renew. Sustain. Energy Rev. 50 (2015) 1004–1012, https://doi.org/10.1016/J.RSER.2015.05.031.
[2] E. Benhelal, G. Zahedi, E. Shamsaei, A. Bahadori, Global strategies and potentials to curb CO_2 emissions in cement industry, J. Clean. Prod. 51 (2013) 142–161, https://doi.org/10.1016/j.jclepro.2012.10.049.
[3] L. Chen, G. Msigwa, M. Yang, A.I. Osman, S. Fawzy, D.W. Rooney, P.S. Yap, Strategies to achieve a carbon neutral society: a review, Environ. Chem. Lett. 1 (2022) 1–34, https://doi.org/10.1007/S10311-022-01435-8/FIGURES/1.
[4] M. Schneider, M. Romer, M. Tschudin, H. Bolio, Sustainable cement production—present and future, Cem. Concr. Res. 41 (2011) 642–650, https://doi.org/10.1016/J.CEMCONRES.2011.03.019.
[5] L. Rosa, V. Becattini, P. Gabrielli, A. Andreotti, M. Mazzotti, Carbon dioxide mineralization in recycled concrete aggregates can contribute immediately to carbon-neutrality, Resour. Conserv. Recycl. 184 (2022), 106436, https://doi.org/10.1016/J.RESCONREC.2022.106436.
[6] F. Belaïd, How does concrete and cement industry transformation contribute to mitigating climate change challenges? Resour. Conserv. Recycl. Adv. 15 (2022), 200084 https://doi.org/10.1016/J.RCRADV.2022.200084.
[7] A SUSTAINABLE FUTURE FOR THE EUROPEAN CEMENT AND CONCRETE INDUSTRY, (n.d.). https://europeanclimate.org/wp-content/uploads/2018/10/AB_SP_Decarbonisation_report.pdf (accessed June 21, 2022).
[8] K.L. Scrivener, V.M. John, E.M. Gartner, Eco-efficient cements: Potential economically viable solutions for a low-CO_2 cement-based materials industry, Cem. Concr. Res. 114 (2018) 2–26, https://doi.org/10.1016/J.CEMCONRES.2018.03.015.
[9] A.M. Kaja, K. Schollbach, S. Melzer, S.R. van der Laan, H.J.H. Brouwers, Q. Yu, Hydration of potassium citrate-activated BOF slag, Cem. Concr. Res. 140 (2021), 106291, https://doi.org/10.1016/j.cemconres.2020.106291.
[10] K. Horii, N. Tsutsumi, Y. Kitano, T. Kato, Processing and reusing technologies for steelmaking slag, Nippon Steel Tech. Rep. (2013).
[11] Slag recycling - recovery, (n.d.). https://www.recovery-worldwide.com/en/artikel/slag-recycling_3528047.html (accessed June 21, 2022).
[12] Y. Jiang, T.C. Ling, C. Shi, S.Y. Pan, Characteristics of steel slags and their use in cement and concrete—A review, Resour. Conserv. Recycl. 136 (2018) 187–197, https://doi.org/10.1016/J.RESCONREC.2018.04.023.
[13] L. De Windt, P. Chaurand, J. Rose, Kinetics of steel slag leaching: Batch tests and modeling, Waste Manag. 31 (2011) 225–235, https://doi.org/10.1016/j.wasman.2010.05.018.
[14] X. Wu, L. Li, Y. Dong, Enrichment and crystallization of vanadium in factory steel slag, Metallurgist 55 (2011) 401–409, https://doi.org/10.1007/S11015-011-9444-0/FIGURES/7.
[15] A. Said, H.P. Mattila, M. Järvinen, R. Zevenhoven, Production of precipitated calcium carbonate (PCC) from steelmaking slag for fixation of CO_2, Appl. Energy 112 (2013) 765–771, https://doi.org/10.1016/J.APENERGY.2012.12.042.
[16] Q. Alam, K. Schollbach, C. van Hoek, S. van der Laan, T. de Wolf, H.J.H.J.H. Brouwers, Q. Alam, C. van Hoek, S. van der Laan, T. de Wolf, H.J.H.J.H. Brouwers, K. Schollbach, C. van Hoek, S. van der Laan, T. de Wolf, H.J.H.J.H. Brouwers, In-depth mineralogical quantification of MSWI bottom ash phases and their association with potentially toxic elements, Waste Manag. submitted, (2019) 1–12. doi:10.1016/j.wasman.2019.01.031.
[17] Q. Alam, K. Schollbach, M. Rijnders, C. van Hoek, S. van der Laan, H.J.H. Brouwers, The immobilization of potentially toxic elements due to incineration and weathering of bottom ash fines, J. Hazard. Mater. 379 (2019), 120798, https://doi.org/10.1016/J.JHAZMAT.2019.120798.
[18] A. Todorut, T. Heput, Broadening of Raw Materials in the Steel Industry, by Recycling and Recovery Wastes, 6 (2012) 1035–1041.
[19] RECYCLING AND ENVIRONMENTAL ISSUES OF METALLURGICAL SLAGS AND SALT FLUXES, (n.d.). https://www.saimm.co.za/Conferences/Slags2004/050_Reuter.pdf (accessed June 21, 2022).
[20] L. Kriskova, Y. Pontikes, F. Zhang, Ö. Cizer, P.T. Jones, K. Van Balen, B. Blanpain, Influence of mechanical and chemical activation on the hydraulic properties of gamma dicalcium silicate, Cem. Concr. Res. 55 (2014) 59–68, https://doi.org/10.1016/j.cemconres.2013.10.004.
[21] P.E. Tsakiridis, G.D. Papadimitriou, S. Tsivilis, C. Koroneos, Utilization of steel slag for Portland cement clinker production, J. Hazard. Mater. (2008), https://doi.org/10.1016/j.jhazmat.2007.07.093.
[22] Y. Li, W. Bin Dai, Modifying hot slag and converting it into value-added materials: a review, J. Clean. Prod. (2018), https://doi.org/10.1016/j.jclepro.2017.11.171.
[23] S. Eloneva, Reduction of CO_2 emissions by mineral carbonation: steelmaking slags and raw material with a pure calcium carbonate end product, 2010.
[24] M. Bodor, R.M. Santos, G. Cristea, M. Salman, Ö. Cizer, R.I. Iacobescu, Y. W. Chiang, K. Van Balen, M. Vlad, T. Van Gerven, Laboratory investigation of carbonated BOF slag used as partial replacement of natural aggregate in cement mortars, Cem. Concr. Compos. 65 (2016) 55–66, https://doi.org/10.1016/J.CEMCONCOMP.2015.10.002.
[25] M. Bodor, R.M. Santos, G. Cristea, M. Salman, Cizer, R.I. Iacobescu, Y.W. Chiang, K. Van Balen, M. Vlad, T. Van Gerven, Utilization of carbonated BOF slag as partial replacement of aggregate in cement mortars, 5th Int. Conf. Accel. Carbonation Environ. Mater. Eng. 2015. (2015) 11–20.
[26] T. Mashifana, N. Sithole, Utilization of fly ash: basic oxygen furnace slag as a raw material in geopolymerization, IOP Conf. Ser. Mater. Sci. Eng. 652 (2019), 012060, https://doi.org/10.1088/1757-899X/652/1/012060.
[27] N.T. Sithole, F. Okonta, F. Ntuli, Development of lightweight construction blocks by alkaline activation of Bof slag, J. Solid Waste Technol. Manag. 45 (2019) 175–185, https://doi.org/10.5276/JSWTM/2019.175.
[28] N.T. Sithole, F. Okonta, F. Ntuli, Mechanical properties and structure of fly ash modified basic oxygen furnace slag based geopolymer masonry blocks, J. Solid Waste Technol. Manag. 46 (2020) 372–383, https://doi.org/10.5276/JSWTM/2020.372.
[29] S. Sandybay, C.S. Shon, A. Tukaziban, D. Syzdykov, I. Orynbassarov, D. Zhang, J. R. Kim, Blended basic oxygen furnace (BOF) slag with ground granulated blast furnace slag (GGBFS) as a pozzolanic material, Mater. Sci. Forum. 1053 (2022) 331–337, https://doi.org/10.4028/P-Q7N2CU.
[30] F. Saly, L. Guo, R. Ma, C. Gu, W. Sun, Properties of steel slag and stainless steel slag as cement replacement materials: a comparative study, J. Wuhan Univ. Technol. Sci. Ed. 2018 336. 33 (2018) 1444–1451. doi: 10.1007/S11595-018-1989-3.
[31] S.Z. Carvalho, F. Vernilli, B. Almeida, M. Demarco, S.N. Silva, The recycling effect of BOF slag in the portland cement properties, Resour. Conserv. Recycl. 127 (2017) 216–220, https://doi.org/10.1016/J.RESCONREC.2017.08.021.
[32] C. van Hoek, J. Small, S. van der Laan, Large-area phase mapping using PhAse recognition and characterization (PARC) software, Micros. Today 24 (2016) 12–21, https://doi.org/10.1017/S1551929516000572.
[33] T. Gao, T. Dai, L. Shen, L. Jiang, Benefits of using steel slag in cement clinker production for environmental conservation and economic revenue generation, J. Clean. Prod. 282 (2021), 124538, https://doi.org/10.1016/J.JCLEPRO.2020.124538.
[34] S. Zhuang, Q. Wang, Inhibition mechanisms of steel slag on the early-age hydration of cement, Cem. Concr. Res. 140 (2021), 106283, https://doi.org/10.1016/j.cemconres.2020.106283.
[35] D.M. Proctor, K.A. Fehling, E.C. Shay, J.L. Wittenborn, J.J. Green, C. Avent, R. D. Bigham, M. Connolly, B. Lee, T.O. Shepker, M.A. Zak, Physical and chemical characteristics of blast furnace, basic oxygen furnace, and electric arc furnace steel industry slags, Environ. Sci. Technol. 34 (2000) 1576–1582, https://doi.org/10.1021/ES9906002.
[36] F. Engström, D. Adolfsson, Q. Yang, C. Samuelsson, B. Björkman, Crystallization behaviour of some steelmaking slags, Steel Res. Int. 81 (2010) 362–371, https://doi.org/10.1002/srin.200900154.
[37] D. Durinck, P.T. Jones, B. Blanpain, P. Wollants, Air-cooling of metallurgical slags containing multivalent oxides, J. Am. Ceram. Soc. 91 (2008) 3342–3348, https://doi.org/10.1111/j.1551-2916.2008.02597.x.
[38] M. Loncnar, M. Zupančič, P. Bukovec, A. Jaklič, The effect of water cooling on the leaching behaviour of EAF slag from stainless steel production, Mater. Tehnol. (2009).
[39] K. Schollbach, M.J. Ahmed, S.R. Laan, The mineralogy of air granulated converter slag, Int. J. Ceram. Eng. Sci. 3 (2021) 21–36, https://doi.org/10.1002/ces2.10074.
[40] A. Wesselsky, O.M. Jensen, Synthesis of pure Portland cement phases, Cem. Concr. Res. (2009), https://doi.org/10.1007/s11368-012-0598-6.
[41] M. Jawad Ahmed, K. Schollbach, S. van der Laan, M. Florea, H.J. Brouwers, A quantitative analysis of dicalcium silicate synthesized via different sol-gel

methods, Mater. Des. 213 (2022), 110329, https://doi.org/10.1016/j.matdes.2021.110329.
[42] A. Cuesta, A. Ayuela, M.A.G. Aranda, Belite cements and their activation, Cem. Concr. Res. 140 (2021), 106319, https://doi.org/10.1016/j.cemconres.2020.106319.
[43] BS EN196-1 Methods of testing cement. Determination of strength., in: BSI, 2016.
[44] Standard, DIN 52,450 Determination of Shrinkage and Expansion of small test specimens, (1985).
[45] B. Pang, Z. Zhou, H. Xu, Utilization of carbonated and granulated steel slag aggregate in concrete, Constr. Build. Mater. 84 (2015) 454–467, https://doi.org/10.1016/j.conbuildmat.2015.03.008.
[46] Q. Wang, P.Y. Yan, S. Han, The influence of steel slag on the hydration of cement during the hydration process of complex binder, Sci. China Technol. Sci. 54 (2011) 388–394, https://doi.org/10.1007/s11431-010-4204-0.
[47] D. Jiao, C. Shi, Q. Yuan, X. An, Y. Liu, H. Li, Effect of constituents on rheological properties of fresh concrete-A review, Cem. Concr. Compos. 83 (2017) 146–159, https://doi.org/10.1016/j.cemconcomp.2017.07.016.
[48] L.R.C. Tavares, J.F.T. Junior, L.M. Costa, A.C. da Silva Bezerra, P.R. Cetlin, M.T.P. Aguilar, Influence of quartz powder and silica fume on the performance of Portland cement, Sci. Reports 2020 101. 10 (2020) 1–15. doi:10.1038/s41598-020-78567-w.
[49] S.Z. Carvalho, F. Vernilli, B. Almeida, M. Demarco, S.N. Silva, The recycling effect of BOF slag in the portland cement properties, Resour. Conserv. Recycl. 127 (2017) 216–220, https://doi.org/10.1016/j.resconrec.2017.08.021.
[50] S.Z. Carvalho, F. Vernilli, B. Almeida, M.D. Oliveira, S.N. Silva, Reducing environmental impacts: the use of basic oxygen furnace slag in portland cement, J. Clean. Prod. 172 (2018) 385–390, https://doi.org/10.1016/j.jclepro.2017.10.130.
[51] S. Kourounis, S. Tsivilis, P.E. Tsakiridis, G.D. Papadimitriou, Z. Tsibouki, Properties and hydration of blended cements with steelmaking slag, Cem. Concr. Res. 37 (2007) 815–822, https://doi.org/10.1016/J.CEMCONRES.2007.03.008.
[52] Y. Wang, P. Suraneni, Experimental methods to determine the feasibility of steel slags as supplementary cementitious materials, Constr. Build. Mater. 204 (2019) 458–467, https://doi.org/10.1016/J.CONBUILDMAT.2019.01.196.
[53] B. Lothenbach, K. Scrivener, R.D. Hooton, Supplementary cementitious materials, Cem. Concr. Res. 41 (2011) 1244–1256, https://doi.org/10.1016/j.cemconres.2010.12.001.
[54] T.H. Lu, Y.L. Chen, P.H. Shih, J.E. Chang, Use of basic oxygen furnace slag fines in the production of cementitious mortars and the effects on mortar expansion, Constr. Build. Mater. 167 (2018) 768–774, https://doi.org/10.1016/j.conbuildmat.2018.02.102.
[55] S. Liu, L. Li, Influence of fineness on the cementitious properties of steel slag, J. Therm. Anal. Calorim. 117 (2014) 629–634, https://doi.org/10.1007/s10973-014-3789-0.
[56] W. Nocuń-Wczelik, Differential calorimetry as a tool in the studies of cement hydration kinetics with sulphate and nitrate solutions, J. Therm. Anal. Calorim. 130 (2017) 249–259, https://doi.org/10.1007/s10973-017-6378-1.
[57] J. Li, Q. Yu, J. Wei, T. Zhang, Structural characteristics and hydration kinetics of modified steel slag, Cem. Concr. Res. 41 (2011) 324–329, https://doi.org/10.1016/j.cemconres.2010.11.018.
[58] T. Hertel, J. Neubauer, F. Goetz-Neunhoeffer, Study of hydration potential and kinetics of the ferrite phase in iron-rich CAC, Cem. Concr. Res. 83 (2016) 79–85, https://doi.org/10.1016/j.cemconres.2016.01.004.
[59] E. Dubina, L. Black, R. Sieber, J. Plank, Functional and Bioceramics Interaction of water vapour with anhydrous cement minerals Interaction of water vapour with anhydrous cement minerals, Adv. Appl. Ceram. Struct. (2013), https://doi.org/10.1179/174367509X12554402491029.
[60] T. Zhang, Q. Yu, J. Wei, J. Li, Investigation on mechanical properties, durability and micro-structural development of steel slag blended cements, J. Therm. Anal. Calorim., Springer (2012) 633–639, https://doi.org/10.1007/s10973-011-1853-6.
[61] L. Chen, H. Wang, K. Zheng, J. Zhou, F. He, Q. Yuan, The mechanism of basic oxygen furnace steel slag retarding early-age hydration of Portland cement and mitigating approach towards higher utilization rate, J. Clean. Prod. 362 (2022), 132493, https://doi.org/10.1016/J.JCLEPRO.2022.132493.
[62] B.Z. Dilnesa, E. Wieland, B. Lothenbach, R. Dähn, K.L. Scrivener, Fe-containing phases in hydrated cements, Cem. Concr. Res. 58 (2014) 45–55, https://doi.org/10.1016/J.CEMCONRES.2013.12.012.
[63] G. Möschner, B. Lothenbach, F. Winnefeld, A. Ulrich, R. Figi, R. Kretzschmar, Solid solution between Al-ettringite and Fe-ettringite (Ca6[Al1 − xFex(OH)6]2(SO_4)3·26H_2O), Cem. Concr. Res. 39 (2009) 482–489, https://doi.org/10.1016/J.CEMCONRES.2009.03.001.
[64] T. Matschei, B. Lothenbach, F.P. Glasser, Thermodynamic properties of Portland cement hydrates in the system CaO–Al_2O_3–SiO_2–$CaSO_4$–$CaCO_3$–H_2O, Cem. Concr. Res. 37 (2007) 1379–1410, https://doi.org/10.1016/J.CEMCONRES.2007.06.002.
[65] F. Han, Z. Zhang, Properties of 5-year-old concrete containing steel slag powder, Powder Technol. 334 (2018) 27–35, https://doi.org/10.1016/j.powtec.2018.04.054.
[66] A.M. Kaja, S. Melzer, H.J.H. Brouwers, Q. Yu, On the optimization of BOF slag hydration kinetics, Cem. Concr. Compos. 124 (2021), 104262, https://doi.org/10.1016/J.CEMCONCOMP.2021.104262.
[67] F. Deschner, B. Lothenbach, F. Winnefeld, J. Neubauer, Effect of temperature on the hydration of Portland cement blended with siliceous fly ash, Cem. Concr. Res. 52 (2013) 169–181, https://doi.org/10.1016/J.CEMCONRES.2013.07.006.
[68] B.Z. Dilnesa, Fe-containing Hydrates and their Fate during Cement Hydration, (2012). doi:10.5075/EPFL-THESIS-5262.
[69] M.J. Ahmed, R. Cuijpers, K. Schollbach, S. Van Der Laan, M. Van Wijngaarden-Kroft, T. Verhoeven, H.J. Brouwers, V and Cr substitution in dicalcium silicate (C_2S) under oxidizing and reducing conditions- Synthesis, reactivity, and leaching behaviour studies, J. Hazard. Mater. (2022), 130032, https://doi.org/10.1016/J.JHAZMAT.2022.130032.
[70] A.J. Hobson, D.I. Stewart, A.W. Bray, R.J.G. Mortimer, W.M. Mayes, M. Rogerson, I.T. Burke, Mechanism of vanadium leaching during surface weathering of basic oxygen furnace steel slag blocks: a microfocus X-ray absorption spectroscopy and electron microscopy study, Environ. Sci. Technol. 51 (2017) 7823–7830, https://doi.org/10.1021/ACS.EST.7B00874/SUPPL_FILE/ES7B00874_SI_001.PDF.
[71] J. Spooren, E. Kim, L. Horckmans, K. Broos, P. Nielsen, M. Quaghebeur, In-situ chromium and vanadium recovery of landfilled ferrochromium and stainless steel slags, Chem. Eng. J. 303 (2016) 359–368, https://doi.org/10.1016/J.CEJ.2016.05.128.
[72] A. van Zomeren, S.R. van der Laan, H.B.A. Kobesen, W.J.J. Huijgen, R.N. J. Comans, Changes in mineralogical and leaching properties of converter steel slag resulting from accelerated carbonation at low CO_2 pressure, Waste Manag. 31 (2011) 2236–2244, https://doi.org/10.1016/j.wasman.2011.05.022.
[73] C.K. Lin, J.N. Chen, C.C. Lin, An NMR and XRD study of solidification/stabilization of chromium with Portland cement and β-C2S, J. Hazard. Mater. 48 (1996) 137–147, https://doi.org/10.1016/0304-3894(95)00154-9.
[74] P. Chaurand, J. Rose, V. Briois, L. Olivi, J.L. Hazemann, O. Proux, J. Domas, J. Y. Bottero, Environmental impacts of steel slag reused in road construction: a crystallographic and molecular (XANES) approach, J. Hazard. Mater. (2007), https://doi.org/10.1016/j.jhazmat.2006.02.060.
[75] Y.L. Chen, Y.C. Lai, C.J. Lin, Y.K. Chang, M.S. Ko, Controlling sintering atmosphere to reduce the hazardous characteristics of low-energy cement produced with chromium compounds, J. Clean. Prod. 43 (2013) 45–51, https://doi.org/10.1016/J.JCLEPRO.2012.12.027.